

1 **Neutral atmosphere temperature change at 90 km, 70°N,**
2 **19°E, 2003-2014**

3

4 **S. E. Holmen¹²³, C. M. Hall² and M. Tsutsumi⁴⁵**

5 [1]{The University Centre in Svalbard, Longyearbyen, Norway}

6 [2]{Tromsø Geophysical Observatory, UiT – The Arctic University of Norway, Tromsø,
7 Norway}

8 [3]{Birkeland Centre for Space Science, Bergen, Norway}

9 [4]{National Institute of Polar Research, Tokyo, Japan}

10 [5]{The Graduate University for Advanced Studies (SOKENDAI), Department of Polar
11 Science, Japan}

12 Correspondence to: S. E. Holmen (siljeh@unis.no)

13

14 **Abstract**

15 Neutral temperatures for 90 km height above Tromsø, Norway, have been determined using
16 ambipolar diffusion coefficients calculated from meteor echo fading times using the
17 Nippon/Norway Tromsø Meteor Radar (NTMR). Daily temperature averages have been
18 calculated from November 2003 to October 2014 and calibrated against temperature
19 measurements from the Microwave Limb Sounder (MLS) on board Aura. The long-term trend
20 of temperatures from the NTMR radar is investigated, and winter and summer seasons are
21 looked at separately. Seasonal variation has been accounted for, as well as solar response,
22 using the F10.7 cm flux as a proxy for solar activity. The temperature change from 2003 to
23 2014 is $-4.1 \text{ K} \pm 1.3 \text{ K/decade}$, while in summer and winter the change is $-0.5 \text{ K} \pm 2.5$
24 K/decade and $-10.6 \text{ K} \pm 3.8 \text{ K/decade}$, respectively. How well suited a meteor radar is for
25 estimating neutral temperatures at 90 km using meteor trail echoes is discussed, and physical
26 explanations behind a cooling trend are proposed.

1 1 Introduction

2 Temperature changes in the mesosphere and lower thermosphere (MLT) region due to both
3 natural and anthropogenic variations cannot be assessed without understanding the dynamical,
4 radiative and chemical couplings between the different atmospheric layers. Processes
5 responsible for heating and cooling in the MLT region are many. Absorption of UV by O₃ and
6 O₂ causes heating, while CO₂ causes strong radiative cooling. Planetary waves (PWs) and
7 gravity waves (GWs) break and deposit heat and momentum into the middle atmosphere and
8 influence the mesospheric residual circulation, which is the summer-to-winter circulation in
9 the mesosphere. Also, heat is transported through advection and adiabatic processes.

10 For decades, it has been generally accepted that increased anthropogenic emissions of
11 greenhouse gases are responsible for warming of the lower atmosphere (e.g. Manabe and
12 Wetherald, 1975), and that these emissions are causing the mesosphere and thermosphere to
13 cool (Akmaev and Fomichev, 2000; Roble and Dickinson, 1989). Akmaev and Fomichev
14 (1998) reported, using a middle atmospheric model, that if CO₂ concentrations are doubled,
15 temperatures will decrease by about 14 K at the stratopause, by about 10 K in the upper
16 mesosphere and by 40-50 K in the thermosphere. Newer and more sophisticated models
17 include important radiative and dynamical processes as well as interactive chemistries. Some
18 model results indicate a cooling rate near the mesopause less than predicted by Akmaev and
19 Fomichev (1998), while others maintain the negative signal (French and Klekociuk, 2011;
20 Beig, 2011a). The thermal response in this region is strongly influenced by changes in
21 dynamics, and some dynamical processes contribute to a warming which counteracts the
22 cooling expected from greenhouse gas emissions (Schmidt et al., 2006).

23 Even though the increasing concentration of greenhouse gases is generally accepted to be the
24 main driver, also other drivers of long-term changes and temperature trends exist, namely
25 stratospheric ozone depletion, long-term changes of solar and geomagnetic activity, secular
26 changes of the Earth's magnetic field, long-term changes of atmospheric circulation and
27 mesospheric water vapour concentration (Laštovička et al., 2012). The complexity of
28 temperature trends in the MLT region and their causes act as motivation for studying these
29 matters further.

30 In this paper, we investigate long-term change of temperatures obtained from the NTMR
31 radar, and we also look at summer and winter seasons separately. In Sect. 2, specifications of
32 the NTMR radar are given, and the theory behind the retrieval of temperatures using

1 ambipolar diffusion coefficients from meteor trail echoes is explained. In Sect. 3, the method
2 behind the calibration of NTMR temperatures against Aura MLS temperatures is explained.
3 Section 4 treats the temperature trend analysis, including the correction for seasonal variation
4 and solar response. The theory and underlying assumptions for the method of determining
5 neutral temperatures from meteor trail echoes and thus how well suited a meteor radar is for
6 estimating such temperatures is discussed in Sect. 5. Also, physical explanations behind the
7 change in temperature are discussed, as well as comparison with other reports on trends.

8 **2 Instrumentation and data**

9 The Nippon/Tromsø Meteor Radar (NTMR) is located at Ramfjordmoen near Tromsø, at
10 69.58°N, 19.22°E. It is operated 24 hours a day, all year round. Measurements are available
11 for more than 90 % of all days since the radar was first operative in November 2003. The
12 meteor radar consists of one transmitter antenna and five receivers and is operating at 30.25
13 MHz. It detects echoes from ionized trails from meteors, which appear when meteors enter
14 and interact with the Earth's neutral atmosphere in the MLT region. The ionized atoms from
15 the meteors are thermalized, and the resulting trails expand in the radial direction mainly due
16 to ambipolar diffusion, which is diffusion in plasma due to interaction with the electric field.
17 Underdense meteors, which are the ones used in this study, have a plasma frequency that is
18 lower than the frequency of the radar, which makes it possible for the radio wave from the
19 radar to penetrate into the meteor trail and be scattered by each electron.

20 Echoes are detected from a region within a radius of approximately 100 km (horizontal
21 space). The radar typically detects around 10000 echoes a day, of which around 200-600
22 echoes are detected per hour at the peak occurrence height of 90 km. Figure 1 shows the
23 vertical distribution of meteor echoes as a function of height, averaged over the time period
24 2003-2014. The number of echoes detected per day allows for a 30 minute resolution of
25 temperature values. The intra-day periodicity in meteor detections by the NTMR radar is less
26 pronounced than that of lower latitude stations and we do not anticipate tidally-induced bias
27 regarding echo rates at specific tidal phases for daily averages. The height resolution and the
28 range resolution are both 1 km, when looking at altitudes around the peak occurrence height.
29 From the decay time of the radar signal we can derive ambipolar diffusion coefficients, D_a :

$$30 \quad D_a = \frac{\lambda^2}{16\pi^2\tau} \quad (1)$$

1 where λ is the radar wavelength and τ is the radar echo decay time. It has been shown that this
2 coefficient also can be expressed in terms of atmospheric temperature and pressure:

$$3 \quad D_a = 6.39 \times 10^{-2} K_0 \frac{T^2}{p} \quad (2)$$

4 where p is pressure, T is temperature, and K_0 is the zero-field reduced mobility factor of the
5 ions in the trail. In this study we use the value for K_0 of $2.4 \times 10^{-4} \text{ m}^2 \text{ s}^{-1} \text{ V}^{-1}$, in accordance
6 with e.g. Holdsworth et al. (2006). Pressure values are derived from atmospheric densities
7 obtained from falling sphere measurements appropriate for 70°N , combining those of Lübken
8 and von Zahn (1991) and Lübken (1999), previously used by e.g. Holdsworth (2006) and
9 Dyrland et al. (2010). These densities do not take into account long-term solar cycle
10 variations.

11 The NTMR radar is essentially identical to the Nippon/Norway Svalbard Meteor Radar
12 (NSMR) located in Adventdalen on Spitsbergen at 78.33°N , 16.00°E . Further explanation of
13 the radar and explanation of theories can be found in e.g. Hall et al. (2002; 2012), Cervera and
14 Reid (2000) and McKinley (1961).

15 Calibration of temperatures derived from meteor echoes with an independent, coinciding
16 temperature series is necessary, according to previous studies (e.g. Hocking, 1999).
17 Temperatures from the NSMR radar have been derived most recently by Dyrland et al.
18 (2010), employing a new calibration approach for the meteor radar temperatures, wherein
19 temperature measurements from the Microwave Limb Sounder (MLS) on the Aura satellite
20 were used instead of the previously used rotational hydroxyl and potassium lidar temperatures
21 from ground-based optical instruments (Hall et al., 2006). Neither ground-based optical
22 observations nor lidar soundings are available for the time period of interest or the location of
23 the NTMR. In this study we therefore employ the same approach as Dyrland et al. (2010),
24 using Aura MLS temperatures to calibrate the NTMR temperatures.

25 NASA's EOS Aura satellite was launched 15 July 2004 and gives daily global coverage
26 (between 82°S and 82°N) with about 14.5 orbits per day. The MLS instrument is one of four
27 instruments on Aura and samples viewing forward along the spacecraft's flight direction,
28 scanning its view from the ground to ~ 90 km every ~ 25 seconds, making measurements of
29 atmospheric temperature, among others (NASA Jet Propulsion Laboratory).

1 Because of a general cooling of most of the stratosphere and mesosphere the last decades due
2 to e.g. increasing concentrations of CO₂ and O₃, the atmosphere has been shrinking, leading to
3 a lowering of pressure surfaces at various altitudes. It is important to distinguish between
4 trends on fixed pressure altitudes and fixed geometric altitudes, since trends on geometric
5 altitudes include the effect of a shrinking atmosphere (Lübken et al., 2013). In this study, we
6 have obtained Aura MLS temperature data (version 3.3) for latitude 69.7°N ± 5.0° and
7 longitude 19.0°E ± 10.0° at 90 km geometric altitude.

8 **3 Calibration of NTMR temperatures**

9 Figure 2 shows daily NTMR temperatures from November 2003 to October 2014, derived
10 from Eqs. (1) and (2), plotted together with Aura MLS temperatures. The Aura satellite
11 overpasses Tromsø at 01-03 UTC and 10-12 UTC, which means that the Aura daily averages
12 are representative for these time windows. It was therefore necessary to investigate any bias
13 arising from Aura not measuring throughout the whole day. A way to do this is to assume that
14 Aura temperatures and NTMR temperatures follow the same diurnal variation and thus
15 investigate the diurnal variation of NTMR temperatures. This was done by superposing all
16 NTMR temperatures by time of day, obtaining 48 values for each day, since the radar allows
17 for a 30-minute resolution.

18 There is an ongoing investigation into the possibility that D_a derived by NTMR can be
19 affected by modified electron mobility during auroral particle precipitation. According to
20 Rees et al. (1972), neutral temperatures in the auroral zone show a positive correlation with
21 geomagnetic activity. It is therefore a possibility that apparent D_a enhancements during strong
22 auroral events do not necessarily depict neutral temperature increase. This matter requires
23 further attention.

24 Investigation of possible unrealistic D_a enhancements was carried out by calculating standard
25 errors of estimated half hourly D_a values:

$$26 \quad se = \frac{\sigma}{\sqrt{ne}} \quad (3)$$

27 where σ is standard deviation and ne is the number of echoes detected by the radar. By
28 inspection and comparison of results between one of the authors (MT) and Satonori Nozawa
29 (private comm.), all half hourly D_a values with a standard error larger than 7 % of the
30 estimated D_a value were excluded from further analysis. This rejection criterion led to that 5.4

1 % of the D_a values were rejected. NTMR temperatures after application of the D_a rejection
2 procedure will henceforward be referred to as D_a -rejected NTMR temperatures.

3 Figure 3 shows monthly averages of the superposed values of D_a -rejected NTMR
4 temperatures as a function of time of day for days coinciding with Aura measurements. It is
5 evident from the figure that the lowest temperatures are in general achieved in the forenoon,
6 which coincides with one of the periods per day when Aura MLS makes measurements over
7 Tromsø.

8 Subtracting the monthly averages of the 00-24 UTC temperatures from the 01-03 UTC and
9 10-12 UTC temperatures gave the estimated biases in Aura daily means due to only sampling
10 during some hours of the day and are given in Fig. 4. The figure shows that by judging by the
11 measurement windows, Aura underestimates the daily mean (00-24 UTC) more during winter
12 than during spring and summer. Note the higher standard deviations in spring and summer
13 compared to winter.

14 The initially obtained Aura temperatures were corrected by adding the biases from Fig. 3 in
15 order to arrive at daily mean temperatures that are representative for the entire day. Also, the
16 Aura temperatures were corrected for “cold bias”. French and Mulligan (2010) reported that
17 Aura MLS temperatures exhibit a 10 K cold bias compared with OH*(6-2) nightly
18 temperatures at Davis Station, Antarctica. A newer study by Garcia-Comas et al. (2014)
19 shows that Aura MLS exhibits a bias compared with several satellite instruments which varies
20 with season. According to their findings, a 10 K correction for cold bias was applied to the
21 Aura summer and winter temperatures (Jun – Aug, Dec - Feb), while a 5 K correction was
22 applied to autumn and spring temperatures (Sep – Nov, Mar – May). The corrected Aura
23 temperatures will henceforward be referred to as local time and cold bias-corrected Aura MLS
24 temperatures.

25 Figure 5 shows a scatterplot of the local time and cold bias-corrected Aura temperatures
26 against the D_a -rejected NTMR temperatures. The red line represents the linear fit ($R^2 = 0.83$)
27 and is described by:

$$28 \quad T_{NTMR} = 0.84T_{Aura} + 32 \quad (4)$$

29 where T_{NTMR} is the D_a -rejected temperature obtained from NTMR, and T_{Aura} is the local time
30 and cold bias-corrected temperature from Aura MLS. Inverting Eq. (4) enabled us to estimate
31 NTMR temperatures calibrated with respect to Aura MLS temperatures. NTMR temperatures

1 were now corrected for the days of measurements coinciding with Aura measurements and are
2 henceforward referred to as MLS-calibrated NTMR temperatures. For calibration of NTMR
3 temperatures from November 2003 to August 2004 (before the start of the Aura MLS
4 dataset), the same equation (Eq. 4) was used, using NTMR Da-rejected temperatures from
5 November 2003 to August 2004 as input instead of T_{Aura} .

6 To estimate the calibration uncertainty, all local time and cold bias-corrected Aura
7 temperatures were subtracted from the MLS-calibrated NTMR temperatures, and the
8 differences were plotted in a histogram with 5 K bins. A Gaussian was fitted to the
9 distribution. The standard deviation of the Gaussian was 11.9 K, which is then considered the
10 overall uncertainty of the calibration. Figure 6 shows the histogram and the fitted Gaussian
11 curve. Finally, Fig. 7 shows the MLS-calibrated NTMR temperatures with uncertainties
12 plotted together with Aura MLS temperatures, corrected for cold and time-of-day
13 measurement bias.

14 **4 Trend analysis**

15 A monthly climatology of the MLS-calibrated NTMR temperatures was obtained by
16 averaging all January, February, etc. values. The seasonal variation is not shown here but
17 reveals a summer minimum of around 150-160 K and a winter maximum of around 200-210
18 K. The monthly values were then subtracted from the daily MLS-calibrated temperatures,
19 obtaining daily residuals independent of seasonal variation.

20 There are several measures of solar variability available, e.g. the F10.7 cm solar radio flux,
21 the sunspot number (SSN), total solar irradiance (TSI), Mg II 280 nm core-to-wing ratio UV-
22 index and the flare index (FI). These indices are considered proxies for solar radiation formed
23 on different altitudes of the solar atmosphere and are highly correlated (Bruevich et al., 2014).
24 In this study we use the F10.7 cm flux as a proxy for solar activity, which is the most
25 commonly used index in middle/upper atmospheric temperature trend studies (e.g. Laštovička
26 et al., 2008; Hall et al., 2012).

27 A 30-day running mean filter was applied to the daily residual temperatures. Figure 8 shows
28 the residuals plotted against corresponding F10.7 cm values. The straight, red line in the
29 figure gave the best linear fit to the daily residuals with a 30-day running mean applied and
30 gave a solar response coefficient of $4.5 \text{ K} \pm 0.3 \text{ K}/100 \text{ SFU}$ ($1 \text{ SFU} = 1 \text{ solar flux unit} = 10^{-22} \cdot$
31 $\text{W} \cdot \text{m}^{-2} \cdot \text{Hz}^{-1}$).

1 From Fig. 8 there appears to be a somewhat non-linear relationship between the temperatures
 2 at 90 km height and the F10.7 cm index. There seems to be a tendency of a less steep increase
 3 in temperatures toward higher F10.7 values. Ogawa et al. (2014) also found a non-linear
 4 relationship between upper atmospheric temperatures and solar activity using EISCAT UHF
 5 radar observations from 200 to 450 km altitude over Tromsø, even though it must be noted
 6 that the altitude range they looked at differs from ours. In Fig. 8 we have therefore also
 7 plotted the quadratic, least-squares fit to the running mean values. Lacking any objective
 8 scientific basis to do otherwise, we chose to fit a 2nd degree polynomial following the
 9 philosophy of Ogawa et al. (2014), although it is conceivable that other functions could be
 10 more suitable. The 2nd degree polynomial gave us a better fit to the residuals ($R^2=0.16$)
 11 compared to the straight line ($R^2=0.03$). We subtracted the solar response from the dataset of
 12 daily, seasonally corrected residuals using this relation:

$$13 \quad T' = T - (a \cdot f10.7^2 + b \cdot f10.7 + c) \quad (5)$$

14 where T' is the new set of residual temperatures with seasonal and solar response subtracted,
 15 T is the residual temperatures with only seasonal variation subtracted, $f10.7$ is the daily F10.7
 16 cm flux corresponding to T , and a , b and c are coefficients of the 2nd degree polynomial ($a=-$
 17 0.0017 , $b=0.41$, $c=-23$).

18 From the new set of temperature residuals we calculated monthly means. This was done to
 19 remove any high-frequency deterministic component, such as that resulting from multi-day
 20 period waves. Finally, the linear trend was found by performing linear regression using a
 21 least-squares fit. The long-term linear temperature trend using monthly means is -4.1 K with a
 22 standard error of 1.3 K/decade. This trend can be considered statistically significant (i.e.
 23 significantly non-zero at the 5 % level), since the uncertainty ($2\sigma = 2.6$ K/decade) is less than
 24 the trend itself (Tiao et al., 1990). Figure 9 shows the linear trend of the monthly values for
 25 the whole dataset, from November 2003 through October 2014. For comparison, the trend
 26 when applying the linear solar response using monthly values is $-4.7 \text{ K} \pm 1.4 \text{ K/decade}$, and
 27 the trend using daily temperature values (applied Eq. 5 for subtraction of solar response) is -
 28 $3.8 \text{ K} \pm 0.6 \text{ K/decade}$.

29 In addition to the average temperature change, we also treated summer and winter seasons
 30 separately. First, trends for each month were investigated using the same approach as for the
 31 average regardless of month. Figure 10 shows the result. Then, averages of November,
 32 December and January, and of May, June and July were made. They were defined as “winter”

1 and “summer”, respectively. The long-term linear winter trend is $-10.6 \text{ K} \pm 3.8 \text{ K/decade}$, and
2 the long-term summer trend is $-0.5 \text{ K} \pm 2.5 \text{ K/decade}$.

3 The trend analysis was also performed without carrying out the D_a rejection procedure
4 explained in Sect. 3. Final results with and without data rejection do not differ significantly
5 considering the calculated uncertainties.

6 **5 Discussion**

7 **5.1 Suitability of a meteor radar for estimation of neutral temperatures at 90** 8 **km height**

9 As explained in Sect. 2, neutral air temperatures derived from meteor trail echoes depend on
10 pressure, p , the zero-field reduced mobility of the ions in the trail, K_0 , and ambipolar diffusion
11 coefficients, D_a . K_0 will depend on the ion composition in the meteor trail, as well as the
12 chemical composition of the atmosphere. The chemical composition of the atmosphere is
13 assumed to not change significantly with season (Hocking, 2004). Unfortunately, the exact
14 content of a meteor trail is unknown. Usually, a value for K_0 between $1.9 \cdot 10^{-4} \text{ m}^2 \text{ s}^{-1} \text{ V}^{-1}$ and
15 $2.9 \cdot 10^{-4} \text{ m}^2 \text{ s}^{-1} \text{ V}^{-1}$ is chosen, depending on what ion one assumes to be the main ion of the
16 trail (Hocking et al., 1997). Even though we in this study have chosen a constant value for K_0
17 of $2.4 \cdot 10^{-4} \text{ m}^2 \text{ s}^{-1} \text{ V}^{-1}$, some variability in K_0 is expected. According to Hocking (2004)
18 variability can occur due to fragmentation of the incoming meteoroid, anisotropy in the
19 diffusion rate, plasma instabilities and variations in the composition of the meteor trail. Using
20 computer simulations, they reported a typical variability in K_0 from meteor to meteor of 27 %
21 and that the variability is most dominant at higher temperatures. Based on this, we cannot rule
22 out sources of error due to the choice of K_0 as a constant, but since we have no possibility to
23 analyse the composition of all meteor trails detected by the radar we have no other choice
24 than to choose a constant value for K_0 .

25 How well ambipolar diffusion coefficients obtained for 90 km altitude are suited for
26 calculating neutral temperatures has previously been widely discussed, e.g. by Hall et al.
27 (2012) for the trend analysis of the Svalbard meteor radar data, but will be shortly repeated
28 here. For calculations of temperatures using meteor radar, ambipolar diffusion alone is
29 assumed to determine the decay of the underdense echoes. Diffusivities are expected to
30 increase exponentially with height through the region from which meteor echoes are obtained
31 (Ballinger et al., 2008; Chilson et al., 1996). Hall et al. (2005) found that this is only the case

1 between ~85 and ~95 km altitude, using diffusion coefficients delivered by NTMR from
2 2004. They found diffusivities less than expected above ~95 km and diffusivities higher than
3 expected below ~85 km. Ballinger et al. (2008) got a similar result using meteor observations
4 over northern Sweden. It has been proposed that processes other than ambipolar diffusion
5 influence meteor decay times. If this is the case it may have consequences for the estimation
6 of temperatures, and therefore it is important to investigate this further.

7 Departures of the anticipated exponential increase with height of molecular diffusion above
8 ~95 km have in previous studies been attributed to gradient-drift Farley-Buneman instability.
9 Farley-Buneman instability occurs where the trail density gradient and electric field are
10 largest. Due to frequent collisions with neutral particles, electrons are magnetised while ions
11 are left unmagnetised, causing electrons and ions to differ in velocity. Electrons then create an
12 electric field perpendicular to the meteor trail, leading to anomalous fading times that can be
13 an order of magnitude higher than those expected from ambipolar diffusion. The minimum
14 altitude at which this occurs depends on the trail altitude, density gradient and latitude, and at
15 high latitudes this altitude is ~95 km. Therefore, using ambipolar diffusion rates to calculate
16 trail altitudes above this minimum altitude may lead to errors of several kilometres, due to
17 that the diffusion coefficients derived from the measurements are underestimated (Ballinger et
18 al., 2008; Dyrud et al., 2001; Kovalev et al., 2008).

19 Reasons for the higher diffusivities than expected according to theory below ~85 km are not
20 completely understood. Hall (2002) proposed that neutral turbulence may be responsible for
21 overestimates of molecular diffusivity in the region ~70-85 km, but this hypothesis was
22 rejected by Hall et al. (2005) due to a lacking correlation between neutral air turbulent
23 intensity and diffusion coefficients delivered by the NTMR radar. Other mechanisms for
24 overestimates of molecular diffusivity include incorrect determination of echo altitude and
25 fading times due to limitations of the radar (Hall et al., 2005).

26 Since the peak echo occurrence height is 90 km and this is also the height at which a
27 minimum of disturbing effects occur, 90 km height is therefore considered the optimal height
28 for temperature measurements using meteor radar. Ballinger et al. (2008) report that meteor
29 radars in general deliver reliable daily temperature estimates near the mesopause using the
30 method outlined in this study, but emphasize that one should exercise caution when assuming
31 that observed meteor echo fading times are primarily governed by ambipolar diffusion. They
32 proposed, after Havnes and Sigernes (2005), that electron-ion recombination can impact

1 meteor echo decay times. Especially can this affect the weaker echoes, and hence can this
2 effect lead to underestimation of temperatures.

3 Determination of temperatures from meteor radar echo times is a non-trivial task, mainly
4 because the calculation of ambipolar diffusion coefficients depends on the ambient
5 atmospheric pressure. By using radar echo decay times to calculate ambipolar diffusion
6 coefficients from Eq. 1, we can from Eq. 2 get an estimate for T^2/p . Input of pressure values
7 into the equation will thus provide atmospheric temperatures. However, measurements of
8 pressure are rare and difficult to achieve at 90 km height, and often one has to rely on model
9 values. Traditionally, pressure values at 90 km have been calculated using the ideal gas law,
10 taking total mass density from atmospheric models, e.g. the MSISE models, where the newest
11 version is NRLMSIS-00. It is hard to verify the pressure values derived from the models
12 because of lack of measurements to compare the model to, and hence using the pressure
13 values may result in uncertainties of estimated atmospheric temperatures. In this study, we
14 obtained pressure values from measurements of mass densities obtained from falling spheres
15 combined with sodium lidar from Andøya (69°N, 15.5°E) (Lübken, 1999; Lübken and von
16 Zahn, 1991). All measurements have been combined to give a yearly climatology, that is, one
17 pressure value for each day of the year. Since Andøya is located in close proximity to Tromsø
18 (approximately 120 km), the pressure values are considered appropriate for our calculations of
19 neutral temperatures. One disadvantage with using pressure values obtained from the falling
20 sphere measurements is that no day-to-day variations are taken into account, only the average
21 climatology.

22 **5.2 Physical explanations for cooling and comparison with other studies**

23 Other studies on long-term mesospheric temperature trends from mid and high latitudes yield
24 mostly negative or near-zero trends. Few studies cover the same time period as ours, and few
25 are from locations close to Tromsø. Hall et al. (2012) reported a negative trend of $-4 \text{ K} \pm 2$
26 K/decade for temperatures derived from the meteor radar from Longyearbyen, Svalbard
27 (78°N, 16°E) at 90 km height over the time period 2001 to 2011, while Holmen et al. (2014)
28 found a near-zero trend for OH* airglow temperatures at ~87 km height over Longyearbyen
29 over the longer time period 1983 to 2013. Offermann et al. (2010) reported a trend of $-2.3 \text{ K} \pm$
30 0.6 K/decade for ~87 km height using OH* airglow measurements from Wuppertal (51°N,
31 7°E). It must be noted that the peak altitude of the OH* airglow layer can vary and thus affect
32 the comparability of OH* airglow temperature trends and meteor radar temperature trends.

1 Winick et al., 2009 report that the OH* airglow layer can range from 75 to >90 km, while the
2 newer study by von Savigny, 2015, indicates that the layer height at high latitudes is
3 remarkably constant from 2003 to 2011. Beig (2011a) reported that most recent studies on
4 mesopause region temperature trends show weak negative trends, which is in line with our
5 results.

6 The estimated solar response coefficient of $4.5 \text{ K} \pm 0.3 \text{ K}/100 \text{ SFU}$ is somewhat smaller than
7 values obtained by Forbes et al. (2014) using SABER data from 2002 through 2013. For
8 latitudes 50°N - 80°N and altitudes 90-100 km solar response coefficients obtained by Forbes
9 et al. are close to $10 \text{ K}/100 \text{ SFU}$. However, Beig (2011b) summarizes results from numerous
10 studies on temperature variability due to solar activity and reports that temperature response
11 in general is $4\text{-}5 \text{ K}/100 \text{ SFU}$ in the upper part of the mesopause. Our result is in line with this.

12 Our results indicate a cooling at 90 km altitude over Tromsø. A general cooling of the middle
13 atmosphere will cause a contraction of the atmospheric column and hence a lowering of upper
14 mesospheric pressure surfaces. The pressure model used as input to Eq. 2 is only seasonally
15 dependent, so a possible trend in pressure at 90 km must be addressed. By looking at Eq. 2, it
16 is evident that if pressure decreases, temperature will decrease even more. By incorporating a
17 decreasing trend in the pressure model will then serve to further strengthen the negative
18 temperature trend we observe.

19 It has been proposed that GWs may be a major cause of negative temperature trends in the
20 mesosphere and thermosphere (Beig, 2011a; Oliver et al., 2013). GWs effectively transport
21 chemical species and heat in the region, and increased GW drag leads to a net effect of
22 cooling above the turbopause (Yigit and Medvedev, 2009). GWs are shown to heat the
23 atmosphere below about 110 km altitude, while they cool the atmosphere at higher altitudes
24 by inducing a downward heat flux (Walterscheid, 1981). However, there are large regional
25 differences regarding trends in GW activity. Hoffmann et al. (2011) found an increasing GW
26 activity in the mesosphere in summer for selected locations, but Jacobi (2014) found larger
27 GW amplitudes during solar maximum and related this to a stronger mesospheric jet during
28 solar maximum, both for winter and summer. Since we have not conducted any gravity wave
29 trend assessment in this study, we cannot conclude that GW activity is responsible for the
30 negative temperature trend, but we cannot rule out its role either. It is not the purpose of this
31 study to analyse the contribution of dynamics to the temperature change we observe.

1 The stronger cooling trend for winter compared to summer is consistent with model studies.
2 Schmidt et al. (2006) and Fomichev et al. (2007) show, using the HAMMONIA and CMAM
3 models, respectively, that a doubling of the CO₂ concentration will lead to a general cooling
4 of the middle atmosphere, but that the high-latitude summer mesopause will experience
5 insignificant change or even slight warming. They propose that this is the result of both
6 radiative and dynamical effects. In summer, the CO₂ radiative forcing is positive due to heat
7 exchange between the cold polar mesopause and the warmer, underlying layers. Also, CO₂
8 doubling alters the mesospheric residual circulation. This change is caused by a warming in
9 the tropical troposphere and cooling in the extratropical tropopause, leading to a stronger
10 equator-to-pole temperature gradient and hence stronger midlatitude tropospheric westerlies.
11 This causes the westerly gravity wave drag to weaken, resulting in decreased adiabatic
12 cooling from a slower ascent of the upper mesospheric circulation.

13 Our results indicate a cooling at 90 km altitude over Tromsø between 2003 and 2014 when
14 deseasonalizing our dataset and calculating trend using all months of the year. At the same
15 time we get quite different trends for winter and summer. We emphasize that this may give a
16 result that may be somewhat difficult to interpret.

17

18 **6 Conclusions**

19 The long-term trend of neutral temperatures at 90 km height derived from the NTMR radar in
20 Ramfjordmoen, Tromsø, with seasonality and solar response subtracted, is $-4.1 \text{ K} \pm 1.3$
21 K/decade . The linear fit between the smoothed daily residuals and corresponding F10.7 cm
22 values gave a solar response coefficient of $4.5 \text{ K} \pm 0.3 \text{ K/100 SFU}$. However, a 2nd degree
23 polynomial gave the best fit to the data and was thus used for correcting the dataset of solar
24 response. When looking at summer and winter seasons separately, the trends are $-0.5 \text{ K} \pm 2.5$
25 K/decade for summer and $-10.6 \text{ K} \pm 3.8 \text{ K/decade}$ for winter.

26 Final results of the trend analysis, both when excluding and including rejection of D_a values
27 due to hypothetical anomalous electrodynamic processes, do not differ significantly. It is
28 reasonable to believe that strong geomagnetic conditions can affect derived temperatures on a
29 short time scale. However, due to the considerable quantity of data employed in this study, it
30 is inconceivable that this effect will change the conclusions regarding trends, as our results
31 also show.

1 90 km is considered the optimal height for retrieval of neutral temperatures using ambipolar
2 diffusion coefficients from NTMR, due to that the peak echo occurrence height detected by
3 the radar is 90 km and that this is also the height at which a minimum of disturbing effects
4 occur. Above ~95 km anomalous fading times that can be an order of magnitude higher than
5 those expected from ambipolar diffusion may be measured, due to gradient-drift Farley-
6 Buneman instability, causing the derived ambipolar diffusion to be underestimated. Below
7 ~85 km higher diffusivities than expected according to theory in which the temperature
8 estimation is based on may be encountered, due to reasons not fully understood.

9 A weak cooling trend is in line with other recent studies on mesopause region temperature
10 trends. A cooling of the middle atmosphere will cause a lowering of upper mesospheric
11 pressure surfaces. By implementing a negative trend in pressure at 90 km into the equation we
12 use for estimating temperatures the negative temperature trend is enhanced, which reinforces
13 our finding of a cooling trend. The most accepted theory behind a cooling of the middle
14 atmosphere is increased greenhouse gas emissions, but also dynamics may play a significant
15 role. Our results yield a more negative trend in winter compared to summer, which may be
16 explained by both radiative and dynamical effects. In summer, a larger heat exchange takes
17 place from atmospheric layers below the cold, polar mesopause. Weakening of gravity wave
18 drag leads to weakening of the mesospheric residual circulation, which counteracts cooling.
19 These effects occur due to increased CO₂ concentrations in the atmosphere, according to
20 model studies.

21 **Acknowledgements**

22 The research for this article was financially supported by The Research Council of Norway
23 through contract 223252/F50 (CoE). NTMR operation was supported by Research Project
24 KP-0 of National Institute of Polar Research. The authors wish to thank Frank Mulligan at
25 Maynooth University, Ireland, for providing the NASA EOS Aura MLS temperatures.

1 References

- 2 Akmaev, R. A. and V. I. Fomichev: Cooling of the mesosphere and lower thermosphere due
3 to doubling of CO₂, *Ann. Geophys.*, 16, 1501-1512, doi: 10.1007/s00585-998-1501-z, 1998.
- 4 Akmaev, R. A. and V. I. Fomichev: A model estimate of cooling in the mesosphere and lower
5 thermosphere due to the CO₂ increase over the last 3-4 decades, *Geophys. Res. Lett.*, 27 (14),
6 2113-2116, doi: 10.1029/1999GL011333, 2000.
- 7 Ballinger, A. P., P. B. Chilson, R. D. Palmer, and N. J. Mitchell: On the validity of the
8 ambipolar diffusion assumption in the polar mesopause region, *Ann. Geophys.*, 26, 3439-
9 3443, 2008.
- 10 Beig, G.: Long-term trends in the temperature of the mesosphere/lower thermosphere region:
11 1. Anthropogenic influences, *J. Geophys. Res. – Space Physics*, 116, A00H11, doi:
12 10.1029/2011JA016646, 2011a.
- 13 Beig, G.: Long-term trends in the temperature of the mesosphere/lower thermosphere region:
14 2. Solar response, *J. Geophys. Res. – Space Physics*, 116, A00H12,
15 doi:10.1029/2011JA016766, 2011b.
- 16 Bruevich, E. A., V. V. Bruevich, and G. V. Yakunina: Changed relation between solar 10.7-
17 cm radio flux and some activity indices which describe the radiation at different altitudes of
18 atmosphere during cycles 21-23, *J. Astrophys. Astr.*, 35, 1-15, 2014.
- 19 Cervera, M. A. and I. M. Reid: Comparison of atmospheric parameters derived from meteor
20 observations with CIRA, *Radio Sci.*, 35 (3), 833-843, doi: 10.1029/1999RS002226, 2000.
- 21 Chilson, P. B., P. Czechowsky, and G. Schmidt: A comparison of ambipolar diffusion
22 coefficients in meteor trains using VHF radar and UV lidar, *Geophys. Res. Lett.*, 23 (20),
23 2745-2748, doi: 10.1029/96gl02577, 1996.
- 24 Dyrland, M. E., C. M. Hall, F. J. Mulligan, M. Tsutsumi, and F. Sigernes: Improved estimates
25 for neutral air temperatures at 90 km and 78°N using satellite and meteor radar data, *Radio*
26 *Sci.*, 45, RS4006, doi: 10.1029/2009rs004344, 2010.
- 27 Dyrud, L. P., M. M. Oppenheim, and A. F. vom Endt: The anomalous diffusion of meteor
28 trails, *Geophys. Res. Lett.*, 28 (14), 2775-2778, 2001.

1 Fomichev, V. I., A. I. Jonsson, J. de Grandpré, S. R. Beagley, C. McLandress, K. Semeniuk,
2 and T. G. Shepherd: Response of the middle atmosphere to CO₂ doubling: Results from the
3 Canadian Middle Atmosphere Model, *J. Climate*, 20, 1121-1144, doi: 10.1175/JCLI4030.1,
4 2007.

5 Forbes, J. M., Zhang, X., and Marsh, D. R.: Solar cycle dependence of middle atmosphere
6 temperatures, *J. Geophys. Res. Atmos.*, 119, 9615-9625, doi:10.1002/2014JD021484, 2014.

7 French, W. J. R. and A. R. Klekociuk: Long-term trends in Antarctic winter hydroxyl
8 temperatures, *J. Geophys. Res.*, 116, D00P09, doi: 10.1029/2011JD015731, 2011.

9 French, W. J. R. and F. J. Mulligan: Stability of temperatures from TIMED/SABER v1.07
10 (2002-2009) and Aura/MLS v2.2 (2004-2009) compared with OH(6-2) temperatures observed
11 at Davis Station, Antarctica, *Atm. Chem. Phys.*, 10, 11439-11446, doi: 10.5194/acp-10-
12 11439-2010, 2010.

13 Garcia-Comas, M., Funke, B., Gardini, A., Lopez-Puertas, M., Jurado-Navarro, A., von
14 Clarmann, T., Stiller, G., Kiefer, M., Boone, C. D., Leblanc, T., Marshall, B. T., Schwartz, M.
15 J., and Sheese, P. E.: MIPAS temperature from the stratosphere to the lower thermosphere:
16 Comparison of vM21 with ACE-FTS, MLS, OSIRIS, SABER, SOFIE and lidar
17 measurements, *Atmos. Meas. Tech.*, 7, 3633-3651, doi:10.5194/amt-7-3633-2014, 2014.

18 Hall, C. M.: On the influence of neutral turbulence on ambipolar diffusivities deduced from
19 meteor trail expansion, *Ann. Geophys.*, 20 (11), 1857-1862, 2002.

20 Hall, C. M., T. Aso, M. Tsutsumi, J. Höffner, F. Sigernes, and D. A. Holdsworth: Neutral air
21 temperatures at 90 km and 70°N and 78°N, *J. Geophys. Res.*, 11, D14105, doi:
22 10.1029/2005JD006794, 2006.

23 Hall, C. M., T. Aso, M. Tsutsumi, S. Nozawa, A. H. Manson, and C. E. Meek: Letter to the
24 editor: Testing the hypothesis of the influence of neutral turbulence on the deduction of
25 ambipolar diffusivities from meteor trail expansion, *Ann. Geophys.*, 23 (3), 1071-1073, 2005.

26 Hall, C. M., M. E. Dyrlund, M. Tsutsumi, and F. J. Mulligan: Temperature trends at 90 km
27 over Svalbard, Norway (78°N 16°E), seen in one decade of meteor radar observations, *J.*
28 *Geophys. Res. – Atmos.*, 117, D08104, doi: 10.1029/2011JD017028, 2012.

1 Havnes, O. and F. Sigernes: On the influence of background dust on radar scattering from
2 meteor trails, *J. Atmos. Solar-Terr. Phys.*, 67, 659-664, doi: 10.1016/j.jastp.2004.12.009,
3 2005.

4 Hocking, W. K.: Temperatures using radar-meteor decay times, *Geophys. Res. Lett.*, 26 (21),
5 3297-3300, doi: 10.1029/1999GL003618, 1999.

6 Hocking, W. K.: Radar meteor decay rate variability and atmospheric consequences, *Ann.*
7 *Geophys.*, 22 (11), 3805-3814, 2004.

8 Hocking, W. K., T. Thayaparan, and J. Jones: Meteor decay times and their use in
9 determining a diagnostic mesospheric temperature-pressure parameter: methodology and one
10 year of data, *Geophys. Res. Lett.*, 24 (23), 2977-2980, doi: 10.1029/97gl03048, 1997.

11 Hoffmann, P., M. Rapp, W. Singer, and D. Keuer: Trends of mesospheric gravity waves at
12 northern middle latitudes during summer, *J. Geophys. Res.*, 116, D00P08, doi:
13 10.1029/2011JD015717, 2011.

14 Holdsworth, D. A., R. J. Morris, D. J. Murphy, I. M. Reid, G. B. Burns, and W. J. R. French:
15 Antarctic mesospheric temperature estimation using the Davis mesosphere-stratosphere-
16 troposphere radar, *J. Geophys. Res. – Atmos.*, 111 (D5), doi: 10.1029/2005jd006589, 2006.

17 Holmen, S. E., M. E. Dyrland, and F. Sigernes: Long-term trends and the effect of solar cycle
18 variations on mesospheric winter temperatures over Longyearbyen, Svalbard (78°N), *J.*
19 *Geophys. Res. – Atmos.*, 119, 6596-6608, doi: 10.1002/2013jd021195, 2014.

20 Jacobi, C.: Long-term trends and decadal variability of upper mesosphere/lower thermosphere
21 gravity waves at midlatitudes, *J. Atmos. Solar-Terr. Phys.*, 118, 90-95, doi:
22 10.1016/j.astp.2013.05.009, 2014.

23 Kovalev, D. V., A. P. Smirnov, and Y. S. Dimant: Modeling of the Farley-Buneman
24 instability in the E-region ionosphere: a new hybrid approach, *Ann. Geophys.*, 26, 2853-2870,
25 2008.

26 Laštovička, J., R. A. Akmaev, G. Beig, J. Bremer, J. T. Emmert, C. Jacobi, M. J. Jarvis, G.
27 Nedoluha, Y. I. Portnyagin, and T. Ulich: Emerging pattern of global change in the upper
28 atmosphere and ionosphere, *Ann. Geophys.*, 26, 1255-1268, 2008.

- 1 Laštovička, J., S. C. Solomon, and L. Qian: Trends in the neutral and ionized upper
2 atmosphere, *Space Sci. Rev.*, 168, 113-145, doi: 10.1007/s11214-011-9799-3, 2012.
- 3 Lübken, F.-J.: Thermal structure of the Arctic summer mesosphere, *J. Geophys. Res. –*
4 *Atmos.*, 104 (D8), 9135-9149, doi: 10.1029/1999JD900076, 1999.
- 5 Lübken, F.-J., Berger, U., and Baumgarten, G.: Temperature trends in the midlatitude summer
6 mesopause, *J. Geophys. Res. Atmos.*, 118, 13347-13360, doi:10.1002/2013JD020576, 2013.
- 7 Lübken, F.-J. and U. von Zahn: Thermal structure of the mesopause region at polar latitudes,
8 *J. Geophys. Res. – Atmos.*, 96 (D11), 20841-20857, doi: 10.1029/91JD02018, 1991.
- 9 Manabe, S. and R. T. Wetherald: The effects of doubling the CO₂ concentration on the
10 climate of a general circulation model, *J. Atmos. Sci.*, 32 (1), 3-15, 1975.
- 11 McKinley, D. W. R.: *Meteor Science and Engineering*, McGraw-Hill, New York, 1961.
- 12 NASA Jet Propulsion Laboratory, EOS Microwave Limb Sounder,
13 <http://mls.jpl.nasa.gov/index-eos-mls.php>, accessed January 2015.
- 14 Offermann, D., P. Hoffmann, P. Knieling, R. Koppmann, J. Oberheide, and W. Steinbrecht:
15 Long-term trends and solar cycle variations of mesospheric temperatures and dynamics, *J.*
16 *Geophys. Res.*, 115, D18127, doi: 10.1029/2009JD013363, 2010.
- 17 Ogawa, Y., T. Motoba, S. C. Buchert, I. Häggström, and S. Nozawa: Upper atmosphere
18 cooling over the past 33 years, *Geophys. Res. Lett.*, 41, 5629-5635, doi:
19 10.1002/2014GL060591, 2014.
- 20 Oliver, W. L., S.-R. Zhang, and L. P. Goncharenko: Is thermospheric global cooling caused
21 by gravity waves?, *J. Geophys. Res. - Space Physics*, 118, 3898-3908, doi:
22 10.1002/jgra.50370, 2013.
- 23 Rees, D., H. Rishbeth, and T. R. Kaiser: Winds and temperatures in the auroral zone and their
24 relations to geomagnetic activity, *Philosophical Transactions of the Royal Society of London.*
25 *Series A, Mathematical and Physical Sciences*, 271, 1217, 563-575, 1972.

1 Roble, R. G. and R. E. Dickinson: How will changes in carbon dioxide and methane modify
2 the mean structure of the mesosphere and thermosphere?, *Geophys. Res. Lett.*, 16 (12), 1441-
3 1444, 1989.

4 Schmidt, H., G. P. Brasseur, M. Charron, E. Manzini, M. A. Giorgetta, and T. Diehl: The
5 HAMMONIA Chemistry Climate Model: Sensitivity of the mesopause region to the 11-year
6 solar cycle and CO₂ doubling, *J. Climate*, 19 (16), 3903-3931, doi: 10.1175/JCLI3829.1,
7 2006.

8 Tiao, G. C., G. C. Reinsel, D. Xu, J. H. Pedrick, X. Zhu, A. J. Miller, J. J. DeLuisi, C. L.
9 Mateer, and D. J. Wuebbles: Effects of autocorrelation and temporal sampling schemes on
10 estimates of trend and spatial correlation, *J. Geophys. Res. – Atmos.*, 95 (D12), 20507-20517,
11 doi: 10.1029/JD095iD12p20507, 1990.

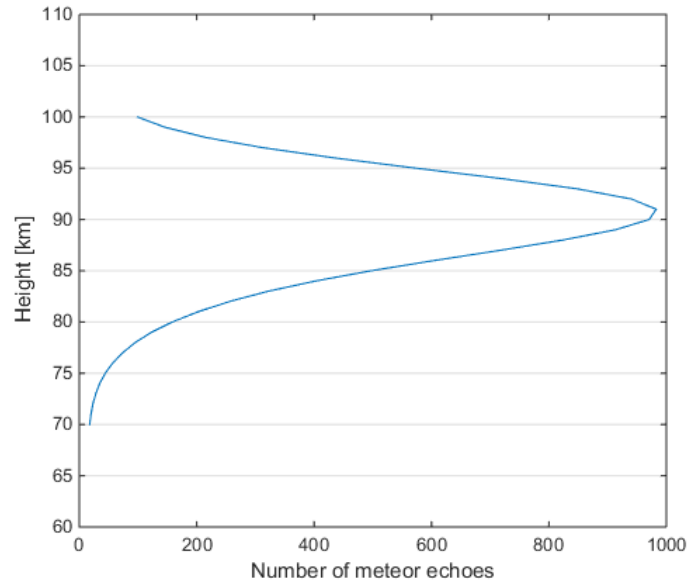
12 von Savigny, C.: Variability of OH(3-1) emission altitude from 2003 to 2011: Long-term
13 stability and universality of the emission rate-altitude relationship, *J. Atmos. Sol.-Terr. Phys.*,
14 127, 120-128, <http://dx.doi.org/10.1016/j.astp.2015.02.001>, 2015.

15 Walterscheid, R. L.: Dynamical cooling induced by dissipating internal gravity waves,
16 *Geophys. Res. Lett.*, 8, 1235-1238, doi: 10.1029/GL008i012p01235.

17 Winick, J. R., P. P. Wintersteiner, R. H. Picard, D. Esplin, M. G. Mlynczak, J. M. Russell III,
18 and L. L. Gordley: OH layer characteristics during unusual boreal winters of 2004 and 2006,
19 *J. Geophys. Res.*, 114, A02303, doi: 10.1029/2008JA013688, 2009.

20 Yigit, E. and Medvedev, A. S.: Heating and cooling of the thermosphere by internal gravity
21 waves, *Geophys. Res. Lett.*, 36, L14807, doi: 10.1029/2009GL038507.

22
23

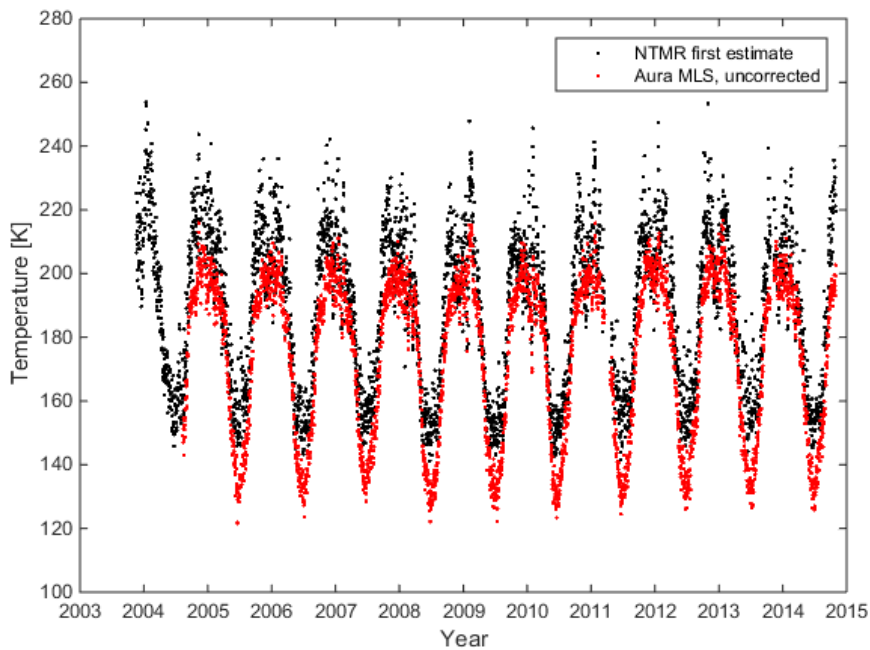


1

2 Figure 1: Vertical distribution of the occurrence of meteor echoes over Tromsø, averaged over
 3 height between 2003 and 2014. The peak occurrence height is just over 90 km altitude.

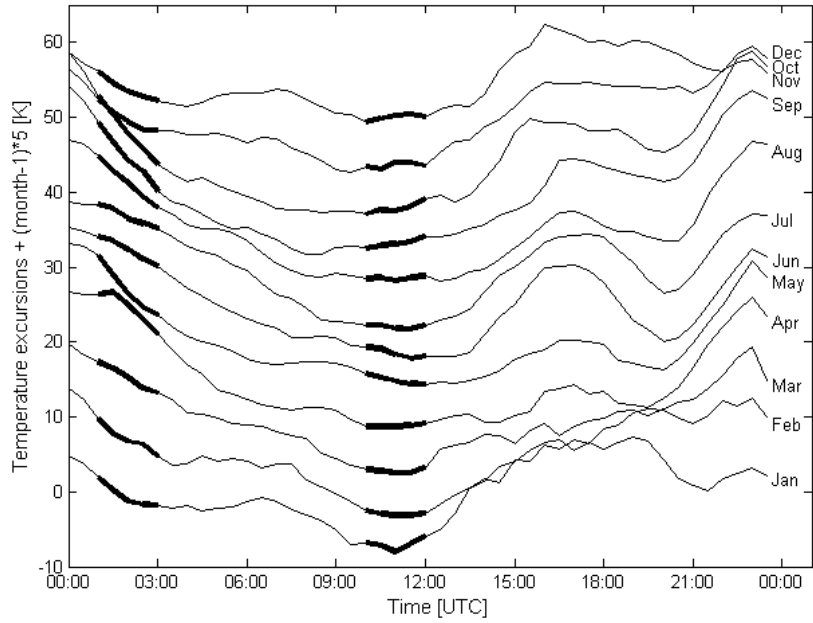
4

5

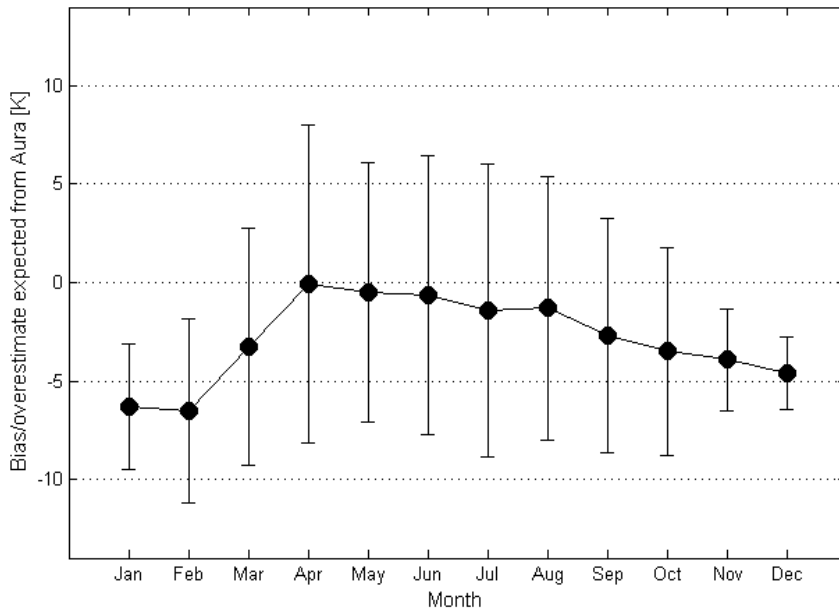


6

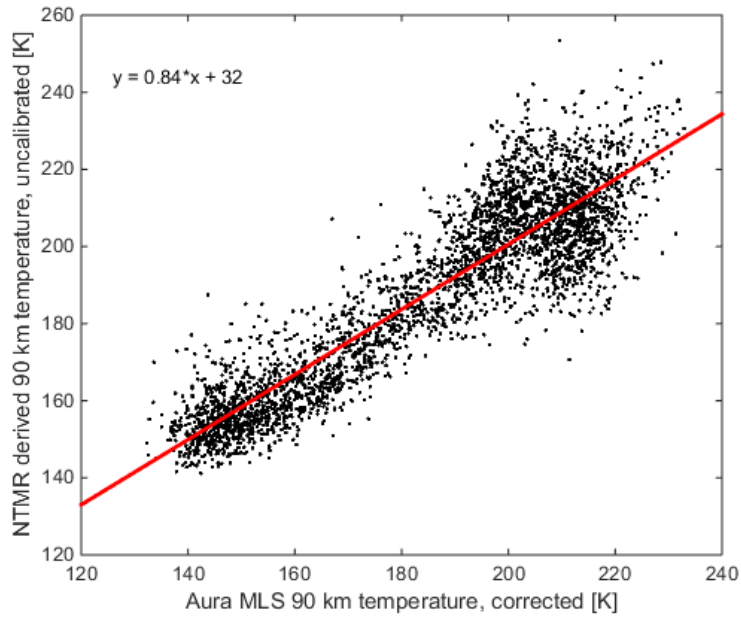
7 Figure 2. Daily values of NTMR temperatures derived from Eqs. (1) and (2), before
 8 correction for high D_a , plotted together with Aura MLS temperatures, before applying any
 9 corrections.



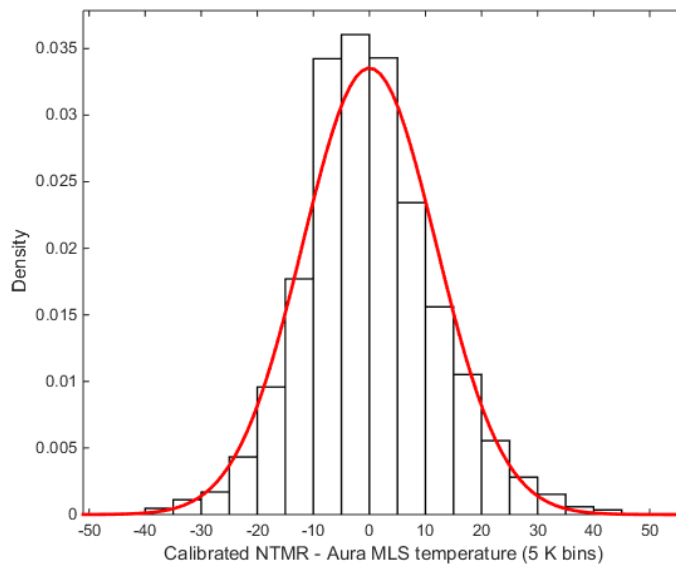
1
 2 Figure 3. Monthly averages of diurnal temperature variation derived from NTMR after
 3 correction for high D_a at 90 km altitude. For clarity time series are displaced by 5 K per
 4 month subsequent to January. The time of day corresponding to when Aura makes
 5 measurements over Tromsø (01-03 UTC and 10-12 UTC) is highlighted.



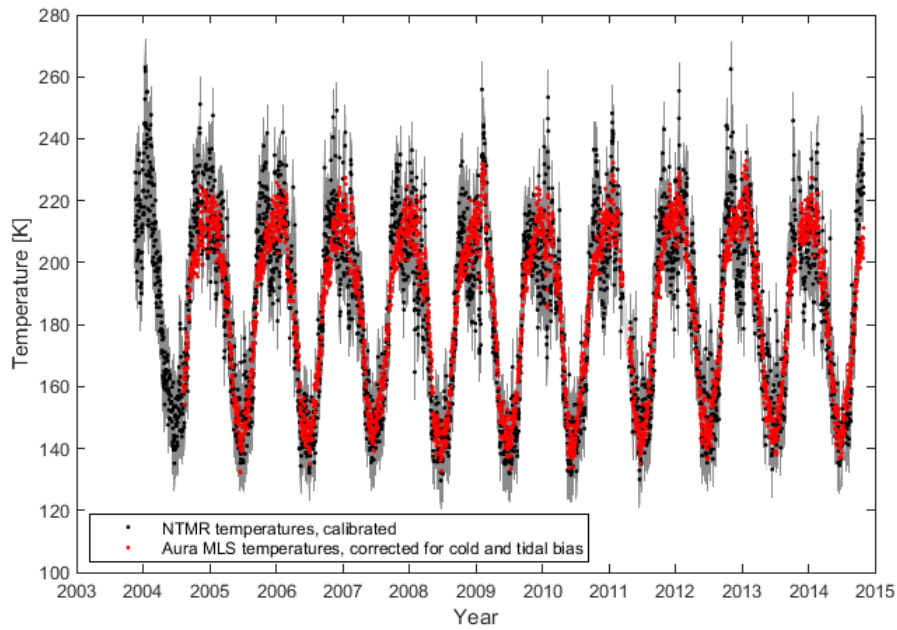
6
 7 Figure 4. Bias in Aura monthly averages due to that Aura MLS only measures between 01
 8 UTC and 03 UTC, and between 10 UTC and 12 UTC. Error bars represent standard
 9 deviations.



1
 2 Figure 5. Scatterplot of Aura temperatures corrected for cold and time-of-day bias against
 3 NTMR D_a -rejected temperatures. The red line represents the linear fit to the data.

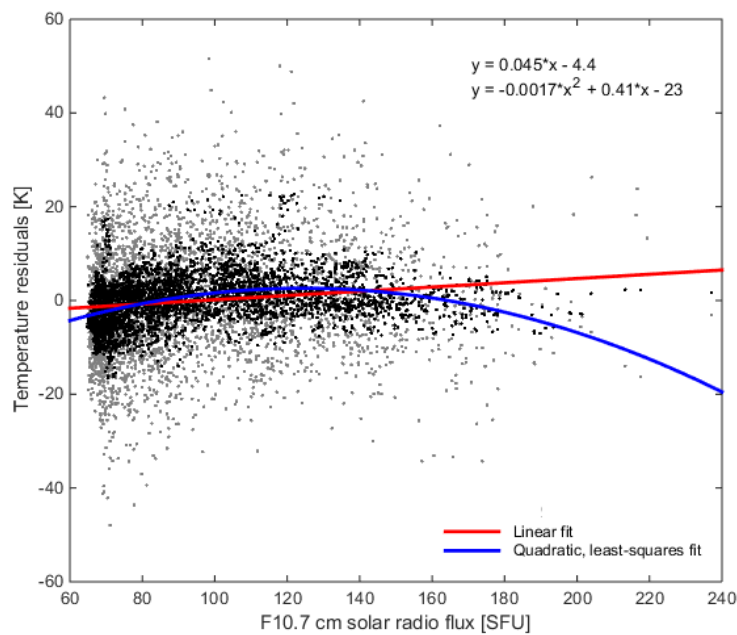


4
 5 Figure 6. Histogram of the differences between MLS-calibrated NTMR temperatures and
 6 local time and cold bias-corrected Aura MLS temperatures. The red curve is a fitted Gaussian
 7 to the distribution.



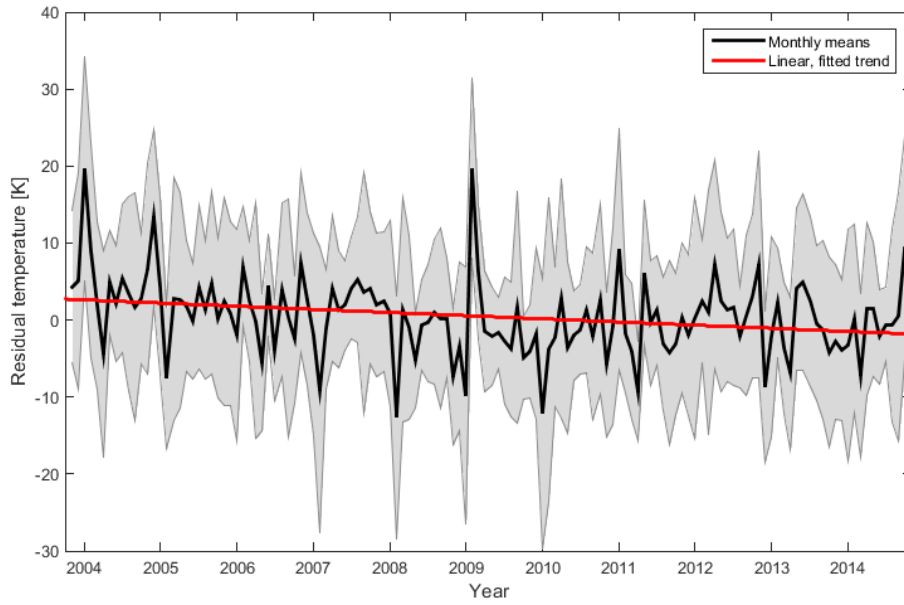
1

2 Figure 7. Daily values of MLS-calibrated NTMR temperatures plotted together with Aura
 3 MLS temperatures corrected for cold and time-of-day bias. The overall calibration uncertainty
 4 is indicated by the grey shading.

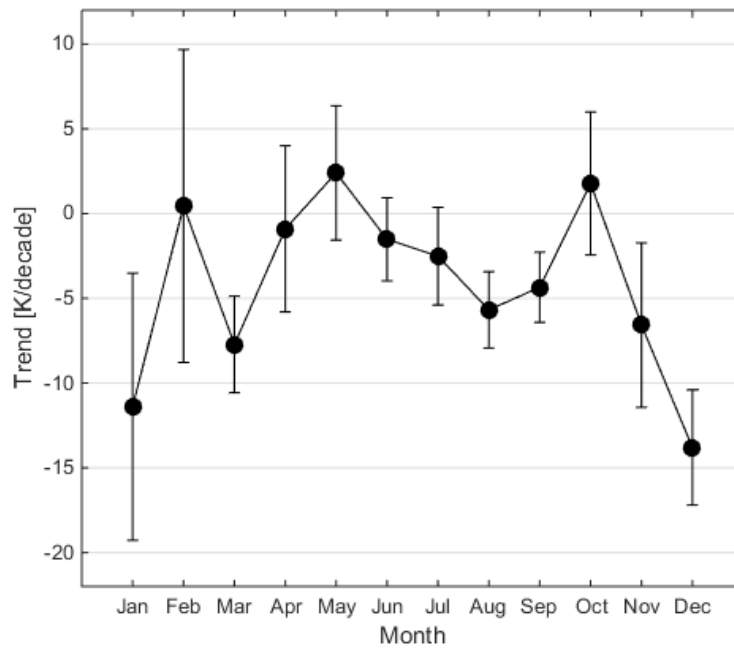


5

6 Figure 8. Scatterplot of daily averaged residuals against the corresponding F10.7 cm solar
 7 flux values. Grey dots are daily residuals, while black dots are the residuals with a 30-day
 8 running mean applied. The red line is the linear fit to the daily residuals with the 30-day
 9 running mean applied, while the blue line is the quadratic, least-squares fit.



1
 2 Figure 9. Monthly means of NTMR residual temperatures, corrected for climatology and solar
 3 response. The grey shading yields standard deviations.



4
 5 Figure 10. Monthly long-term temperature trends at 90 km altitude over Tromsø. Standard
 6 deviations are given as error bars.